Strong Anisotropy and Diameter Effects on the Low-Field Mobility of Silicon Nanowires

Neophytos Neophytou and Hans Kosina
Institute for Microelectronics, Techinical University of Vienna
Gußhausstraße 27-29/E360, A-1040, Vienna, Austria
e-mail: {neophytou|kosina }@iue.tuwien.ac.at

***Abstract*— We describe a method to couple the $sp^3d^5s^*$-spin-orbit-coupled (SO) atomistic tight-binding (TB) model and linearized Boltzmann transport theory for the calculation of low-field mobility in Si nanowires (NWs). We consider scattering mechanisms due to phonons and surface roughness. We perform a simulation study of the low-field mobility in n-type and p-type Si NWs of diameters from 3nm to 12nm, in the [100], [110] and [111] transport orientations. We find that the NW mobility is a strong function of orientation and diameter. This is a consequence of the large variations in the electronic structure with geometry and quantization. Especially in the case of p-type [111] and [110] NWs, large phonon-limited mobility improvements with diameter scaling are observed.**

Keywords – Si nanowires; low-field mobility; Boltzmann transport; bandstructure; MOSFETs; $sp^3d^5s^*$ tight binding model; atomistic;

I. INTRODUCTION

Silicon NW devices are among the potential candidates for future electronic [1], thermoelectric and optoelectronic device applications. NW devices with channels of just a few nanometers in diameter have already been demonstrated [2, 3, 4, 5]. NWs provide the possibility of utilizing a variety of transport orientations and cross sectional length scales as additional degrees of freedom for performance optimization [6]. To properly investigate the influence of these geometrical features on the electronic structure and performance of the NWs, sophisticated models beyond the effective mass approximation are necessary, that can accurately capture effects on the atomistic scale. Utilizing atomistic models, on the other hand, restricts the size of the structures that need to be simulated to a few nanometers. In this work, the $sp^3d^5s^*$-spin-orbit-coupled tight-binding model is utilized to compute the electronic structure of the NWs [7]. This TB model is a compromise between fully ab-initio methods and more simplified effective mass approximation methods. Relatively large NW diameters can be accounted (up to D=12nm in this work, 5500 atoms in the simulation domain). The model has been calibrated extensively to experimental data in various occasions to ensure accuracy and transferability of the results [8]. In this work we describe a methodology to couple TB with linearized Boltzmann transport for calculating the low-field mobility in NWs [9, 10]. We include scattering mechanisms due to acoustical and optical phonons and surface roughness scattering (SRS). We find that the NW mobility is a strong function of orientation and diameter. Mobility variations/improvements of up to 4X compared to bulk values in the cases of p-type [111] and [110] NWs are observed with diameter reduction.

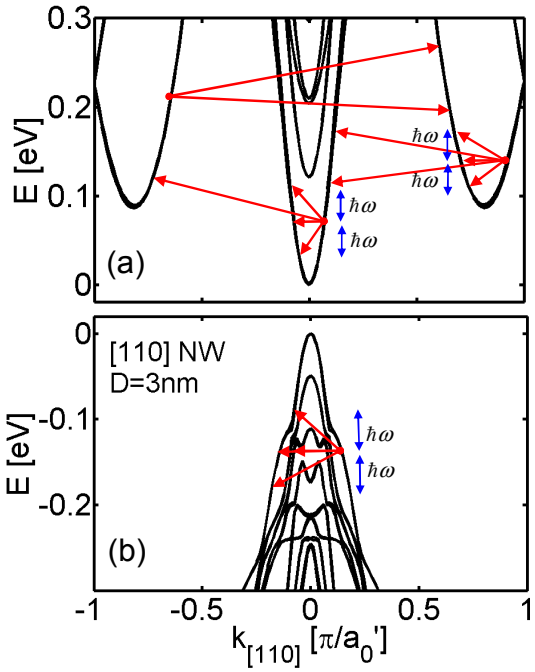

Figure 1. Dispersions of the [110] NW with D=3nm, with intra-valley and inter-valley scattering mechanisms indicated. (a) n-type. (b) p-type.

II. APPROACH

Typical NW electronic structures calculated using the $sp^3d^5s^*$-SO tight-binding model are shown in Fig. 1 for [110] oriented, cylindrical NW of D=3nm. Figure 1a and Fig. 1b show the conduction and valence bands, respectively. We use the atomistic electronic structures (together with their eigenfunctions) in linearized Boltzmann transport calculations including all relevant scattering processes as indicated in Fig. 1. We included elastic, inelastic, intra-band, inter-band, intra-valley and inter-valley processes as appropriate. We follow the bulk scattering processes when we select the final scattering state, i.e. for the conduction band we allow intra-valley elastic scattering and inter-valley inelastic. For phonon scattering all

978-1-61284-418-3/11/$26.00 © 2011 IEEE

relevant *f*- and *g*-processes are included. For the valence band we allow intra-valley/inter-valley elastic and inelastic transitions. The electrical low-field conductivity follows from the linearized Boltzmann equation as:

$$\sigma = q_0^2 \int_{E_0}^{\infty} dE \left(-\frac{\partial f(E)}{\partial E} \right) \Xi(E), \tag{1}$$

where $\Xi(E)$ is the so called transport distribution function defined as [11]:

$$\begin{aligned} \Xi(E) &= \frac{1}{A} \sum_{k_x,n} v_n^2(k_x) \tau_n(k_x) \delta(E - E_n(k_x)) \\ &= \frac{1}{A} \sum_{n} v_n^2(E) \tau_n(E) g_{1D}^n(E). \end{aligned} \tag{2}$$

In Eq. (2) $v_n(E) = \frac{1}{\hbar} \frac{\partial E_n}{\partial k_x}$ is the bandstructure velocity, $\tau_n(k_x)$ is the momentum relaxation time for a carrier with wavenumber k_x in subband n,

$$g_{1D}^n(E_n) = \frac{1}{2\pi\hbar} \frac{1}{v_n(E)} \tag{3}$$

is the density of states for the 1D subbands (per spin), and A is the cross sectional area of the NW. The carrier mean free path (MFP) and the mobility are defined as: $\lambda = 2\pi\hbar\Xi(E)/M$ [12] and $\mu = \sigma / q_0 N$, respectively, where M is the number of conducting channels and N is the carrier concentration. The transition rate for a carrier in an initial state k_x in subband n to a final state k_x' in subband m is extracted from the numerically calculated dispersions and waveform overlaps using Fermi's Golden Rule:

$$S_{n,m}(k_x, k_x') = \frac{2\pi}{\hbar} \left| H_{k_x', k_x}^{m,n} \right|^2 \delta(E_m(k_x') - E_n(k_x) - \Delta E). \tag{4}$$

For computational efficiency, both in terms of CPU time and memory we use the following approximations: i) We use bulk, dispersionless phonons, and ignore the effects of phonon confinement. Instead, we employ higher deformation potential values, more appropriate for NWs, which can at a certain degree account for the effects of confinement. $D_{ODP}^{holes} = 13.24\text{x}10^{10}$ eV / m, $D_{ADP}^{holes} = 5.34$ eV, and $D_{ADP}^{electrons} = 9.5$ eV are used from Refs [13, 14], which are more relevant for NWs. All other parameters are taken from Ref. [15]. ii) For SRS we derive the transition rate strength from the shift in the band edges due to changes in the confinement length scale as described by Uchida *et* al [16]. This treatment ignores several Coulomb related effects, as well as the wavefunction deformations at the interfaces. However, it has been described in several works, both theoretical and experimental, that the shift in the band edge is the dominant SRS mechanism in ultra scaled channels [16, 17]. iii) When computing the waveform overlaps we use the probability density of each state, as in a single orbital model (equivalent to the effective mass), rather than the actual wavefunctions, although we still keep their k_x-dependence. This reduces the memory needed in the computation by 20X, allowing simulations of large NW cross sections with only slightly reduced accuracy. We note that these approximations are commonly employed in the literature, and will affect our results at most quantitatively. The qualitative behavior in terms of geometry and orientation effects we describe originates from electronic structure and will only be slightly affected by these approximations. The entire procedure is described in detail in [9].

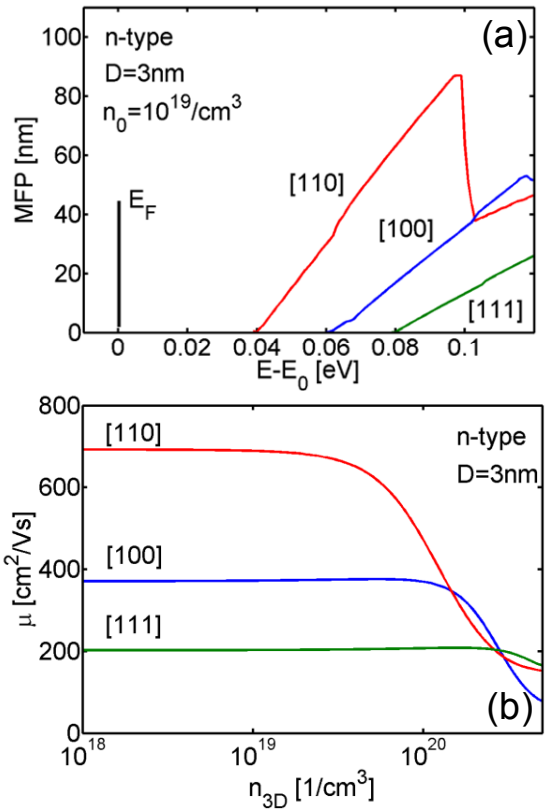

Figure 2. Transport quantities for electrons in NWs of *D*=3nm in different transport orientations. (a) Phonon-limited mean-free-path versus energy. (b) Phonon-limited low-field mobility versus carrier concentration.

III. Results and Discussion

Figure 2a shows the energy-dependent phonon-limited MFP (lowest subband shown only) for n-type NWs of *D*=3nm in the [100] (blue), [110] (red) and [111] (green) transport orientations. Figure 2b shows the phonon-limited mobility of these NWs versus carrier concentration. A large orientation dependence is observed. The [110] NWs have the largest MFPs and mobility, almost 2X and 3X larger than those of the [100] and [111] NWs, respectively. The MFP depends linearly on the TD function. The orientation behavior of mobility is determined in two ways: i) With the slope/magnitude of MFP(E), which is inversely proportional to the transport mass, and ii) with the separation of the MFP(E) function from the Fermi level at a specific carrier concentration (same as the separation of the band edge from the Fermi level). The higher the slope is, the higher are the MFP and the mobility after integration in energy. The closer to the Fermi level the MFP(E) resides (or the band edges), the higher is the mobility

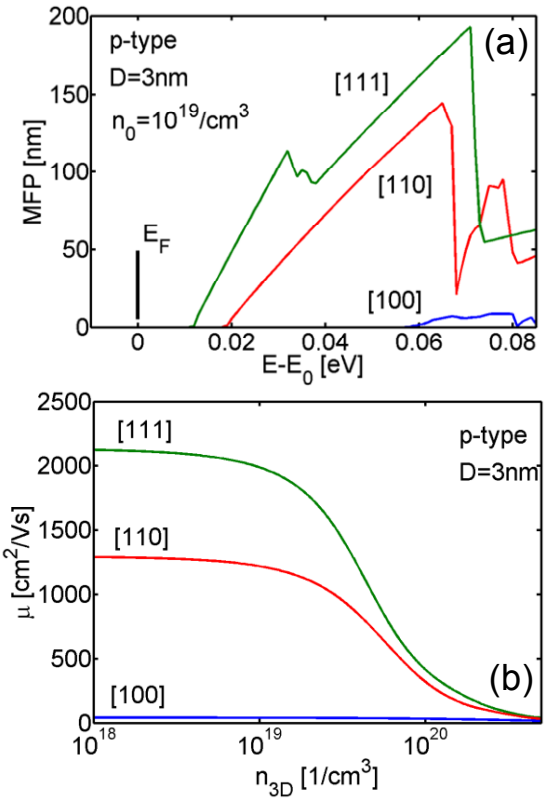

Figure 3. Transport quantities for holes in NWs of *D*=3nm in different transport orientations. (a) Phonon-limited mean-free-path versus energy. (b) Phonon-limited Low-field mobility versus carrier concentration.

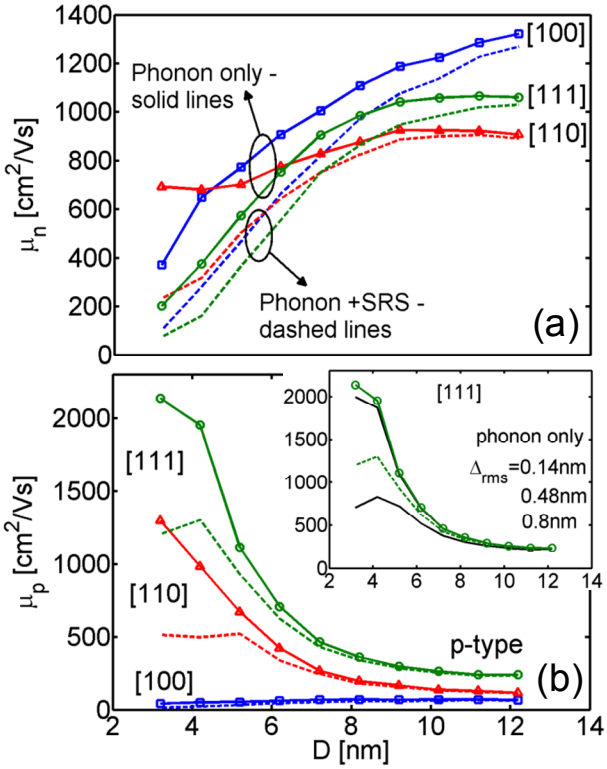

Figure 4. The low-field mobility for NWs in [100] (blue), [110] (red) and [111] (green) transport orientations versus the NWs' diameter. Phonon-limited results are shown by solid and phonon plus SRS results by dashed lines (Δ_{rms}=0.48nm, L_C=1.3nm). (a) Electron mobility. (b) Hole mobility. Inset of (b): The hole [111] NW mobility for different roughness Δ_{rms} values. The data in (b) are same as in [10].

after energy integration over the Fermi distribution. The distance of the Fermi level from the subband mimima at a specific carrier concentration is determined by the DOS effective mass of the subbands and their degeneracy. In 1D, the DOS effective mass is the transport mass as well. The lighter the mass and the lower the degeneracy, the closer the TD function will reside to the Fermi level. As we presented in earlier work [8], the effective electron mass of the [110] NWs reduces with diameter scaling (from $0.19m_0$ to $0.16m_0$ at D=3nm), whereas those of the [100] and [111] NWs increase (from $0.19m_0$ and $0.43m_0$ to $0.27m_0$ and $0.55m_0$ respectively).

Therefore, although at larger diameters, when the electronic structure approaches to bulk Si, all valleys reside at the same energy level independently of orientation. As the diameters are reduced, the variation in the effective masses forces the band edges to be placed in different positions, which affects the MFP and mobility of each NW channel. As a result, for *D*=3nm NWs, at a given energy the MFP for electrons is much longer for the [110] NWs, followed by that of the [100] NW, and finally that of the [111] NW. The orientation dependence of mobility follows the same trend. For the [110] NWs, the phonon limited MFP can reach up to 80nm at $2k_BT$ above the band edge.

Figure 3a and 3b show the phonon-limited MFPs and mobilities for the p-type NWs of *D*=3nm in the three orientations. In this case anisotropy is even larger, with the [111] NW and secondly the [110] NW having large MFPs and mobilities, whereas the [100] p-type NW has very low MFP and mobility. Interestingly, the hole MFP of the [111] and [110] NWs reaches, respectively, up to 200nm and 150nm for energies of $2k_BT$ above the band edges. On the other hand, the MFP for holes in the [100] NWs remains low, indicating poor performance for this NW orientation. The hole mobility for the [111] NW reaches up to 2200 cm^2/Vs, which is even larger than the mobility of bulk electrons, and much larger than the mobility of bulk holes. The [110] NW also indicates high performance compared to the bulk hole mobility. In this case the low-field phonon-limited mobility reaches 1300 cm^2/Vs. On the other hand, the [100] NWs have a significantly lower mobility. These large differences in the performance of the p-type NWs in the different orientations originate from the differences in their effective masses. In the case of the [111] and [110] NWs the effective mass is lower than $0.2m_0$, whereas in the case of the [100] NW, it remains as high as ~m_0 [10, 18]. Finally, we note that both for n-type and p-type NWs, the mobility anisotropy is reduced significantly at higher carrier concentrations (<$10^{20}/cm^3$). As one moves to higher energies, the bands begin to look more alike, and the anisotropy is reduced.

The low-field mobility is a strong function of diameter as well. Figure 4a and 4b show the mobilities for electrons and holes, respectively, as a function of the NWs' diameter (low

carrier concentration values). Phonon-limited results are indicated by solid lines, whereas phonon plus surface roughness scattering (SRS) results are indicated by dashed lines. For electrons in Fig. 4a, as the diameter is reduced, the mobility drops by 4X-6X due to the stronger phonon and SRS processes. For larger diameters the [100] NWs perform better, whereas at *D*=3nm the [110] orientation is beneficial. As the diameter is reduced, the degradation is the least for the [110] NW (especially the phonon-limited one) because the reduction in the effective mass compensates for the detrimental effect of enhanced scattering.

For holes the anisotropy and diameter dependence is much stronger (Fig. 4b) [10]. For [111] and [110] p-type NWs, the phonon-limited mobility increases by almost 8X with diameter scaling. This originates from bandstructure modifications due to confinement [4]. As explained in Refs. [6, 10, 19], the electronic structure of the [111] and [110] NWs undergoes significant changes upon quantization. The curvature significantly increases because the bands that form the dispersion of these NWs are "picked" from high curvature regions of the bulk heavy-hole bandstructure. This results in lower effective masses, larger carrier velocities, reduced scattering rates, and finally significant improvements in hole mobility and MFPs. The same effect is responsible for the reduction in the effective masses of the n-type [110] NW with diameter reduction, but that effect is much weaker [8]. No mobility improvement is observed in that case (Fig. 4a), but the detrimental effect of enhanced scattering with diameter reduction is partially compensated.

In the case of p-type [111] and [110] NWs, even when SRS is considered, mobility enhancements can still be achieved with diameter scaling. The inset of Fig. 4b shows the [111] NW hole mobility for various roughness Δ_{rms} values. Mobility enhancements are still possible even with Δ_{rms} values as high as 0.8nm. The mobility of the [100] p-type NW, on the other hand, is much lower and drops as the diameter is reduced.

IV. Conclusion

In this computational study, we present a method to couple electronic structures extracted from the $sp^3d^5s^*$ atomistic TB model with linearized Boltzmann transport calculations. We include phonon and surface roughness scattering mechanisms. We analyze the low-field mobility and mean-free-path for n-type and p-type NWs in [100], [110] and [111] transport orientations and diameters from *D*=3nm to *D*=12nm. We find that the mobility of Si NWs is a strong function of both diameter and orientation. In the case of n-type NWs, mobility reduces with diameter scaling. The [100] orientation yields the highest electron mobility at large diameters and the [110] orientation at smaller diameters. For p-type NWs, the mobility of the [111] and [110] NWs largely increases as the diameter is reduced. The [111] and secondly the [110] orientations have the highest hole mobility at all diameter ranges, whereas the [100] has a much lower mobility. We show that in general, the confinement length scale and geometrical features of nanoscale channels can act as additional degrees of freedom in designing their properties, and in some cases largely improved performance can be achieved.

Acknowledgment

This work was supported by the Austrian Climate and Energy Fund, contract No. 825467.

References

[1] ITRS Public Home Page. http://www.itrs.net/reports.html

[2] N. Singh et. al., "Ultra-narrow silicon nanowire gate-all-around CMOS devices: Impact of diameter, channel-orientation and low temperature on device performance," *In. Elec. Dev. Meeting*, 2006.

[3] K. H. Cho, *et* al., "Experimental evidence of ballistic transport in cylindrical gate-all-around twin silicon nanowire metal-oxide-semiconductor field-effect transistors," *Appl. Phys. Lett*., 92, 052102, 2008.

[4] M. Kobayashi and T. Hiramoto, "Experimental study on quantum confinement effects in silicon nanowire metal-oxide-semiconductor field-effect transistors and single-electron transistors," *J. Appl. Phys.*, 103, 053709, 2008.

[5] Bangsaruntip *et* al., *VLSI Symposium*, 2010.

[6] Neophytou *et* al., "Subband engineering for p-type silicon ultra-thin layers for increased carrier velocities: An atomistic analysis," *J. Appl. Phys.*, vol. 107, p. 113701, 2010.

[7] T. B. Boykin, G. Klimeck, and F. Oyafuso, "Valence band effective-mass expressions in the $sp^3d^5s^*$ empirical tight-binding model applied to a Si and Ge parametrization," *Phys. Rev. B*, vol. 69, pp. 115201-115210, 2004.

[8] N. Neophytou, A. Paul, M. Lundstrom, and G. Klimeck, "Bandstructure effects in silicon nanowire electron transport," *IEEE Trans. Elect. Dev.*, vol. 55, no. 6, pp. 1286-1297, 2008.

[9] N. Neophytou and H. Kosina, "Effects of confinement and orientation on the thermoelectric power factor of silicon nanowires," *Phys. Rev. B*, 83, 245305, 2011.

[10] N. Neophytou and H. Kosina, "Large enhancement in hole velocity and mobility in p-type [110] and [111] silicon nanowires by cross section scaling: An atomistic analysis," *Nano Lett.*, vol. 10, no. 12, pp. 4913-4919, 2010.

[11] G. D. Mahan et al., *PNAS*, 93, pp. 7436-7439, 1996.

[12] C. Jeong *et* al., "On Landauer versus Boltzmann and full band versus effective mass evaluation of thermoelectric transport coefficients," *J. Appl. Phys*., 107, 023707, 2010.

[13] A. K. Buin, A. Verma, A. Svizhenko, and M. P. Anantram, "Significant Enhancement of Hole Mobility in [110] Silicon Nanowires Compared to Electrons and Bulk Silicon," *Nano Lett.*, vol. 8, no. 2, pp. 760-765 (2008).

[14] A. K. Buin, A. Verma, and M. P. Anantram, "Carrier-phonon interaction in small cross-sectional silicon nanowires," *J. Appl. Phys.*, vol. 104, p. 053716, 2008.

[15] M. Lundstrom, "Fundamentals of Carrier Transport," Cambridge University Press, 2000.

[16] K. Uchida and S. Takagi, "Carrier scattering induced by thickness fluctuation of silicon-on-insulator film in ultrathin-body metal–oxide–semiconductor field-effect transistors," *Appl. Phys. Lett.*, vol. 82, no. 17, pp. 2916-2918 (2003).

[17] M. Saitoh, S. Kobayashi, and K. Uchida, *Int. Elec. Dev. Meeting, IEDM*, pp. 711-714 (2007).

[18] N. Neophytou, A. Paul, and G. Klimeck, "Bandstructure effects in silicon nanowire hole transport," *IEEE Trans. Nanotechnol.*, vol. 7, no. 6, pp. 710-719, 2008.

[19] N. Neophytou and G. Klimeck, "Design space for low sensitivity to size variations in [110] PMOS nanowire devices: The implications of anisotropy in the quantization mass," *Nano Lett.*,vol. 9, no. 2, pp. 623-630, 2009.